JOURNAL OF MATERIALS SCIENCE **35** (2000) 1939–1947

Effect of surface treatment upon the pull-out behaviour of aramid fibres from epoxy resins

R. J. YOUNG, D. J. BANNISTER, A. J. CERVENKA, I. AHMAD
Manchester Materials Science Centre, UMIST/University of Manchester, Grosvenor Street, Manchester M1 7HS, UK
E-mail: robert.young@umist.ac.uk

A detailed study has been undertaken of the pull-out behaviour of aramid fibres with different surface characteristics from blocks of an epoxy resin matrix. The fibres employed had either no surface treatment (HM), a standard surface finish (HMF) or had been treated with a special epoxy-based adhesion-activating finish (HMA). The point-to-point variation of axial fibre strain along the fibres both inside and outside of the resin matrix has been determined from stress-induced Raman band shifts. This has enabled the distribution of interfacial shear stress along the fibre/matrix interface to be determined and, in combination with scanning electron microscope analysis of the specimens following pull-out testing, the failure mechanisms to be elucidated. It is found that pull out of the HM fibre takes place by a debond propagating along the fibre/matrix interface at a low level of interfacial shear stress. The HMF fibre showed better adhesion to the epoxy matrix with pull out occurring in a complex manner through both separation of the fibre skin and failure at the fibre/finish interface. No evidence of debonding was found for the HMA fibre and failure occurred by fracture of the fibre at the point where it entered the resin block.

1. Introduction

It is widely acknowledged that the improvement of aramid composite performance is dependent on a basic understanding of the mechanisms that effect the fibre/matrix adhesion and its subsequent failure [1–3]. The success of the single-fibre pull-out test in conjunction with Raman spectroscopy to model the interfacial behaviour of an aramid/epoxy composite interface has already been demonstrated [4, 5]. The application of a partial-debonding model to the strain profiles obtained from Raman measurements allowed the quantification of interfacial characteristics τ_i and τ_s, where τ_i is the interfacial frictional shear stress and τ_s is the interfacial shear strength. Raman spectroscopy can quantify the effects of the surface treatment on the shear stresses at the fibre/matrix interface but it cannot determine the nature of the failure, i.e. adhesive or cohesive. Therefore scanning electron microscopy has been used to examine the failure surfaces at the entrance of the fibre into the resin and of the extracted fibre. The objective of this study is to identify the pull-out failure characteristics of an aramid fibre with differing surface treatments and to elucidate the effects of surface modification on composite performance.

2. Background

2.1. Surface modification of aramid fibres

In order to improve the adhesion to epoxy matrices, one can chemically modify the surface of aramid fibres to increase the concentration of reactive functional groups. For improved adhesion, only the outermost few molecular layers should react as this will minimise mechanical damage which might lead to cohesive failure modes [6]. Promising results have been reported for the chemical modification of poly(*p*-phenylene terephthalamide) (PPTA) aramid fibre surfaces by plasma treatments designed to provide a functional group for covalent bonding with epoxy resin [7]. The authors showed that stable reactive amine functional groups on surfaces of PPTA filaments can improve the interlaminar strength of epoxy-based laminates, suggesting the formation of covalent bonds between surface amino groups and the epoxy network at the interface. With this consideration in mind Wu and Tesoro [8] introduced functional groups on the surface of PPTA by polymer analogous reactions, under conditions that would not impair the mechanical properties of the fibre. Their results showed similar results to those of Allred *et al.* [7] with a markedly improved interlaminar strength.

Penn *et al.* [9] tested the assumption that reactive groups at the surface of an aramid fibre increased the interfacial adhesion by the formation of covalent bonds with the epoxy matrix. They concluded that reactive functional groups on a fibre surface did not necessarily form covalent bonds with a reactive matrix. However, the fact that there was no chemical reaction between the reactive surface groups and the epoxy molecule in their experiments, precluded the improvement of fibre-matrix adhesion by a covalent bonding mechanism.

Further research by Penn and Chou [10] focused on attaching carefully-designed molecular chains directly to the surface of an aramid fibre prior to making the fibre-matrix adhesive bond. The chemical structures of the attached chains were selected to exploit one or more of the fundamental mechanisms of adhesion [11]. They found that depending upon the structure of the attached chains, the adhesive performance between the fibre and an epoxy resin could be significantly affected. Short inert chains did not alter the fibre-matrix adhesion. Chains capable of chemical bonding with the matrix increased the adhesion significantly. Long polar chains also enhanced the adhesion by an amount that increased with chain length.

The importance of polar-physical interactions in interfacial adhesion was demonstrated by Mahy *et al.* [12] who studied adhesion mechanisms between Twaron fibre and epoxy, using model epoxy monomers. The properties of the epoxy monomers, e.g. molecular dimensions, rigidity and polarity, were varied systematically. A difunctional amine was used as a hardener. Sophisticated surface analysis techniques were used to characterise the surface chemical composition and the results were compared to mechanical bundle pull-out experiments. It was demonstrated that the nature of the interfacial adhesion between fibre and (model) epoxy was dominated by polar-physical interactions, presumably involving the ether-oxygen moeities.

Whilst the debate over the presence of covalent bonding continues, Kalantar and Drzal [13] concluded from their experiments on the aramid/epoxy interface that both the mechanical and chemical interactions present at the carbon/epoxy interface are absent at the aramid/epoxy interface. From the observation of fibrillar separation within the fibre surface by transmission electron microscopy, it was postulated that the fibre skin morphology may be the limiting factor in achieving greater interfacial adhesion with aramid fibres.

2.2. Single-fibre pull-out test

2.2.1. Elastic stress transfer

Piggott [14, 15] has analysed elastic stress transfer for a pull-out specimen with one end of a fibre embedded over a length, L_e, in a resin block with the fibre gripped at the point where it leaves the resin. Application of a strain to the fibre, ε_{app}, in order to extract the fibre from the polymer matrix creates a stress distribution within the embedded region of the fibre that declines with a distance x from the polymer surface. If it assumed that there is no bonding across the fibre end, then the distribution of strain in a fibre of radius, r, is given by [14, 15]

$$\varepsilon_f = \varepsilon_{app}\frac{\sinh[n(L_e - x)/r]}{\sinh[ns]} \quad (1)$$

where ε_f is the axial strain in the embedded region of the fibre at distance x from the resin surface, and s is the fibre aspect ratio L_e/r. The parameter n is given by

$$n^2 = \frac{E_m}{E_f}\frac{1}{\ln(R/r)}\frac{1}{(1+\nu_m)} \quad (2)$$

where E_m is the matrix modulus, E_f is the fibre modulus, ν_m is the matrix Poisson's ratio and $\ln(R/r)$ can be considered to be a volume fraction parameter [15].

The corresponding interfacial shear stress, τ, is obtained from the consideration of the equilibrium of forces exerted on a differential fibre element of length dx [16]:

$$\tau = E_f\frac{d\varepsilon_f}{dx}\frac{r}{2} \quad (3)$$

Differentiation of Equation 1 and substitution into Equation 3 yields:

$$\tau = \frac{n}{2}E_f\varepsilon_{app}\frac{\cosh[n(L_e - x)/r]}{\sinh[ns]} \quad (4)$$

2.2.2. Partial debonding model

The elastic and debonding theories proposed by Piggott [14, 15] can be modified to model the partial debonding behaviour of single-fibre composites. A partial debonding theory for pull-out has been developed [5] following the work of Desaeger *et al.* [17] who were concerned with the application of a partial debonding theory to the fragmentation test.

For the totally debonded situation, Piggott [14, 15] assumed that at a distance $x = L_e$ the strain in the fibre falls linearly to zero. However, in the partially debonded case the assumption that the strain distribution in the debonded region is defined by the embedded length is not valid. From Raman strain profiles to be shown later it is clear that the linear decrease in strain in the debonded region is defined by an imaginary point $x = i$. The distribution of fibre strain in the debonded region is given by integrating Equation 3 as

$$\varepsilon_f = \frac{2\tau_i(i - x)}{rE_f} \quad (5)$$

In the fragmentation test Piggott assumed that debonding occurred over a distance $mL_e/2$ from the fibre ends, with $0 < m < 1$. For epoxy/aramid pull-out specimens consisting of a single fibres in epoxy resin blocks, debonding is found to initiate at the polymer surface ($x = 0$), where the fibre enters the resin [4, 5, 18]. It can be assumed, therefore, that debonding occurs over a distance $(1 - m)L_e$ from the polymer surface.

In the zone of perfect adhesion, Equation 1 and the continuity of axial stress at $x = (1 - m)L_e$ yield

$$\varepsilon_f = \frac{2\tau_i}{rE_f}[i - (1 - m)L_e]\frac{\sinh[n(mL_e - x)/r]}{\sinh[nms]} \quad (6)$$

Differentiating Equation 6 and substituting into Equation 3 yields

$$\tau = \frac{n\tau_i}{r}[i - (1 - m)L_e]\frac{\cosh[n(mL_e - x)/r]}{\sinh[nms]} \quad (7)$$

Equations 6 and 7 define the axial strain and interfacial shear stress distributions in the region of the composite

where there is no debonding. The corresponding distribution of axial fibre strain in the debonded region is given by Equation 5 where the interfacial shear stress has a constant value of τ_i, the interfacial frictional shear stress [5].

3. Experimental procedure

3.1. Materials

3.1.1. Fibres

The fibres used in this study were Twaron® 1055 high modulus fibres supplied by Akzo Nobel Central Research, Arnhem, The Netherlands. Three variants of the fibre were employed:

- HM Twaron High Modulus As-spun fibre,
- HMF Twaron High Modulus Finished,
- HMA Twaron High Modulus Adhesion Activated.

The HMF Twaron fibre contains a polyalkylene glycol finish, which is a component containing polar glycol and apolar alkylene molecules. In the case of the HMA Twaron fibres a similar finish is mixed with an epoxy (glycidylether of glycerol) and a hardener (piperazine), and then applied after a maturation of several hours. Twaron high modulus fibres have a tensile modulus of ∼105 GPa, a tensile strength of ∼2.8 GPa and a diameter of ∼12 μm [19].

3.1.2. Matrix

The matrix material was a two-part, cold-curing epoxy resin consisting of 100 parts by weight of LY5052 resin and 38 parts by weight of HY5052 hardener, both obtained from Ciba Geigy. The resin contains a rigid novolak base and a low molecular weight reactive diluent of butane-1,4-diol diglycidyl ether. The commercial hardener is a mixture of diamine including primarily isophorone diamine (35–45%) and 4,4 diamino-3-3′-dimethyl-dicyclohexylmethane (50–60%). The resin was cured at room temperature for 7 days, has a Young's modulus of ∼3 GPa and a shear yield stress of ∼43 MPa [20].

3.2. Preparation of single-fibre pull-out (SFPO) specimens

The SFPO specimens were prepared in silicone rubber moulds approximately 10 mm × 10 mm × 3 mm as described in detail elsewhere [5]. A segment of the rubber, approximately 5 mm × 5 mm, was removed from the centre of the mould with an adapted razor blade. The moulds contained a cut at about 0.5 mm deep in the wall to allow the introduction of a single fibre. The desired embedded length was obtained by drawing the fibre through the cut. The cavity was filled with epoxy resin and was cured at room temperature (25 ± 2 °C) for 7 days. After curing, the sample was removed carefully by deforming the mould.

Optically-flat smooth surfaces of the specimens were obtained by placing the individual mould on glass slides covered with release paper. A smooth top surface combined with a sharp 90° corner between the top and the side surfaces were essential in the production of good specimens for Raman spectroscopy. Specimens were prepared with embedded lengths of between 600 and 1000 μm with a free fibre length of approximately 40 mm.

3.3. Raman spectroscopy

The SFPO specimens were fixed individually to small glass slides with the free-fibre length cemented between two small pieces of card as described elsewhere [5]. The specimens were mounted on a 'Minimat' miniature materials straining rig (Polymer Laboratories, UK), which was subsequently placed on the stage of an optical microscope connected to a Spex monochromator. Raman spectra were obtained from the aramid fibres, both in air and within the epoxy resin, using the 632.8 nm red line of a 15 mW helium-neon laser focused to a 5 μm spot on the surface of the fibre. A highly sensitive charge-coupled device was used to collect Raman spectra using an exposure time of 5 s. The peak position of the strain sensitive 1610 cm^{-1} Raman band [4, 5] was used to map the fibre strain profiles at various levels of applied strain.

3.4. Scanning electron microscopy

Scanning electron microscopy was undertaken upon both the aramid fibres and pull-out specimens using a Philips 505 SEM operated at 10 or 20 kV. The specimens were sputter coated with a thin layer of gold to render them conductive. Fibres that had been extracted completely from the resin block were mounted on to stubs for SEM analysis. The remaining epoxy blocks and pull-out specimens for which complete fibre extraction had not been obtained before fibre fracture were examined in the region where the fibre entered the resin.

4. Results and discussion

4.1. Fibre characterisation

Table I shows the dependence of the position of the 1610 cm^{-1} aramid Raman band upon tensile strain for single Twaron filaments cemented to the surface of a Perspex beam deformed on a four-point bending rig [21] with the surface strain monitored by a strain gauge. The as-spun (HM) and surface finished (HMF) fibres exhibit a similar Raman shift of $d\Delta\nu/d\varepsilon = 5.0$ $cm^{-1}/\%$. The activated fibre (HMA) shows a slightly lower strain dependence with a Raman

TABLE I Strain dependence of the 1610 cm^{-1} aramid Raman band for the three classes of Twaron fibre

Fibre	Raman band shift ($d\nu/d\varepsilon$) $cm^{-1}/\%$
HM	5.1 ± 0.2
HMF	5.0 ± 0.4
HMA	4.6 ± 0.2

shift of $d\Delta\nu/d\varepsilon = 4.6$ cm^{-1}/%. The difference in Raman sensitivity of the HMA fibre may be a consequence of the conditions encountered in the adhesion activation process [12].

The surface topography of the Twaron fibres was investigated using scanning electron microscopy (SEM) and typical micrographs are shown in Fig. 1. The as-spun (HM) fibre (Fig. 1a) was found to have a very smooth surface compared to the activated (HMF—Fig. 1b) and finished (HMA—Fig. 1c) fibres [19, 22].

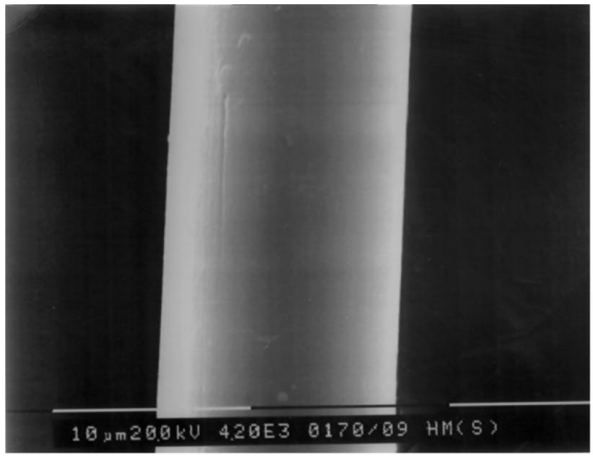

(a)

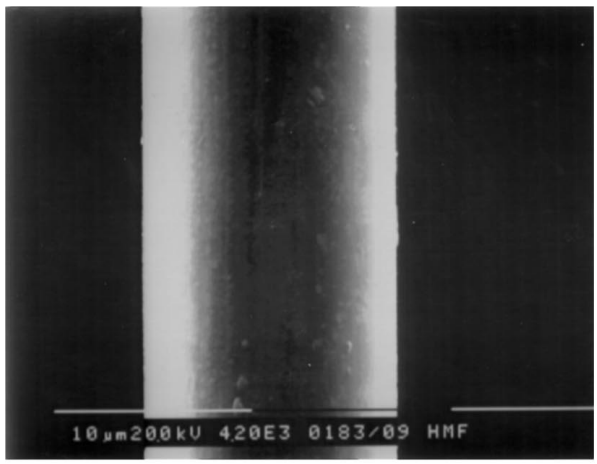

(b)

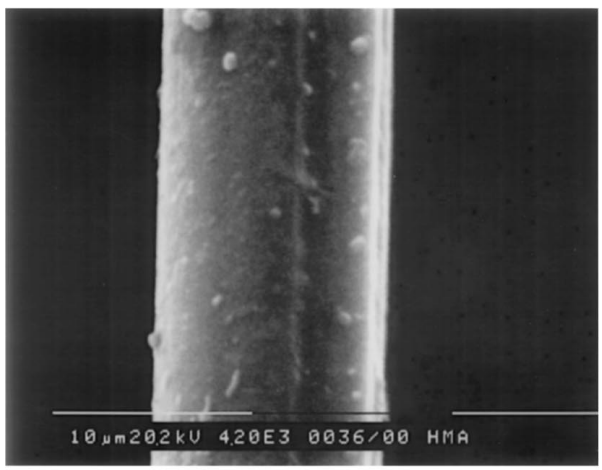

(c)

Figure 1 Scanning electron micrographs of the surface topographies of the Twaron high modulus fibres. (a) HM, (b) HMF and (c) HMA.

The increase in surface roughness is expected to improve all adhesion mechanisms [3] in addition to any chemical interactions. Fibre diameters were determined from the SEM micrographs giving values similar to those obtained by Andrews [21] of 11.8, 12.1, and 12.0 μm for HM, HMF and HMA fibres respectively.

4.2. Single fibre pull-out tests

Several pull-out samples for each surface treatment were examined using Raman spectroscopy as they underwent quasi-static pull-out from an epoxy resin block. The results for a typical sample from each batch are presented here. To enable modelling of the strain profiles, the data were adjusted to eliminate the small residual strains produced in the fibre on manufacture of the specimens. This will have no significant effect on the results of the modelling because the determination of the interfacial parameters τ_i and τ_s depends on the gradients of the strain profiles and not the absolute strain values.

4.2.1. As-spun HM fibres

Fig. 2a shows the axial strain profiles along a Twaron high modulus as-spun fibre of embedded length $L_e = 600$ μm undergoing pull-out from the epoxy resin.

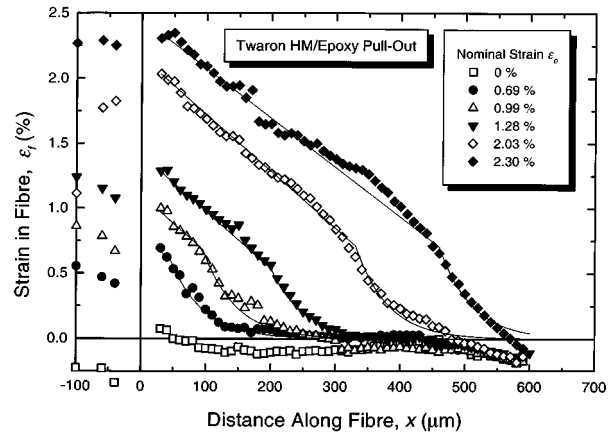

(a)

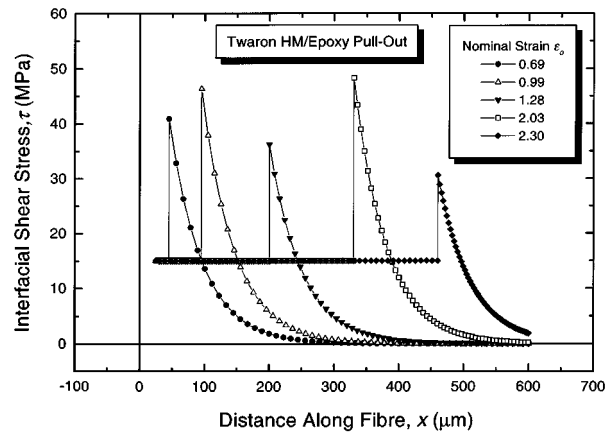

(b)

Figure 2 (a) Experimentally-measured and theoretically-predicted variation of fibre strain with distance along the fibre at different nominal strain levels for the Twaron HM/epoxy specimen with $L_e = 600$ mm undergoing partial debonding. (b) Distributions of interfacial shear stress at different nominal strain levels derived from the data in Fig. 2a.

The plot shows the progress of a linear strain region along the interface as the nominal applied strain is increased from $\varepsilon_o = 0.69\%$ to $\varepsilon_o = 2.30\%$. The data can be fitted to the partial debonding theory [5] (Equations 6 and 7) showing a good correlation for all levels of applied strain. Disparity between the theory and the experimental data was observed in the region of the fibre end as the effects of the free end became significant. This might be expected considering the complex stress state arising at this singularity and the boundary conditions used to develop the theory. The value of applied strain corresponding to total debonding could be quantified in this experiment. This is because the fibre was extracted totally on the application of the increment of strain above $\varepsilon_o = 2.30\%$.

Fig. 2b shows the corresponding interfacial shear stress distributions for the HM sample derived through Equation 3 from the theoretical curves fitted to the fibre strain profile in Fig. 2a. As the debond progresses along the interface the frictional shear stresses remain approximately constant ($\tau_i \sim 15$ MPa). The maximum shear stress values, τ_{max}, at the bond/debond transition vary between 31 MPa and 48 MPa and this can be taken to be the interfacial shear strength, τ_s. The average maximum shear stress value for this experiment, τ_{max}^{avg}, is ~ 40 MPa; this is comparable to the shear yield stress of the resin [19].

Several other Raman experiments were performed using the Twaron HM fibres and the data obtained were analysed in an identical manner to that described above. The interfacial parameters extracted from the Raman plots for the specimen used in Fig. 2 and from four other nominally identical pull-out experiments are summarised in Table II. Statistical analysis of the data indicates that the average maximum shear stress value for the five different specimens, τ_{max}^{avg}, is 40.1 ± 5.0 MPa and the average frictional shear stress τ_i^{avg} is 10.3 ± 3.3 MPa.

TABLE II Interfacial data from 5 Twaron HM fibre/epoxy resin pull-out specimens

Specimen	ε_o (%)	m (μm)	τ_i (MPa)	τ_{max} (MPa)
1	0.69	45	15.0	40.9
	0.99	95	15.0	46.4
	1.28	200	15.0	36.2
	1.66	280	12.0	43.1
	2.03	330	15.0	48.3
	2.30	430	13.0	47.7
2	2.03	230	10.0	42.6
	1.32	330	10.0	43.9
	1.90	575	9.0	44.0
	2.10	770	7.5	42.6
3	0.77	200	4.0	37.5
	1.04	290	4.5	45.4
	1.34	440	6.0	39.7
4	0.70	40	9.0	31.8
	0.83	60	9.0	33.8
	1.17	130	11.0	34.5
	1.48	200	10.5	36.8
5	1.10	65	9.0	34.0
	1.32	140	10.0	36.6
	1.71	350	11.0	36.4
Average			**10.3**	**40.1**
SD			**3.3**	**5.0**

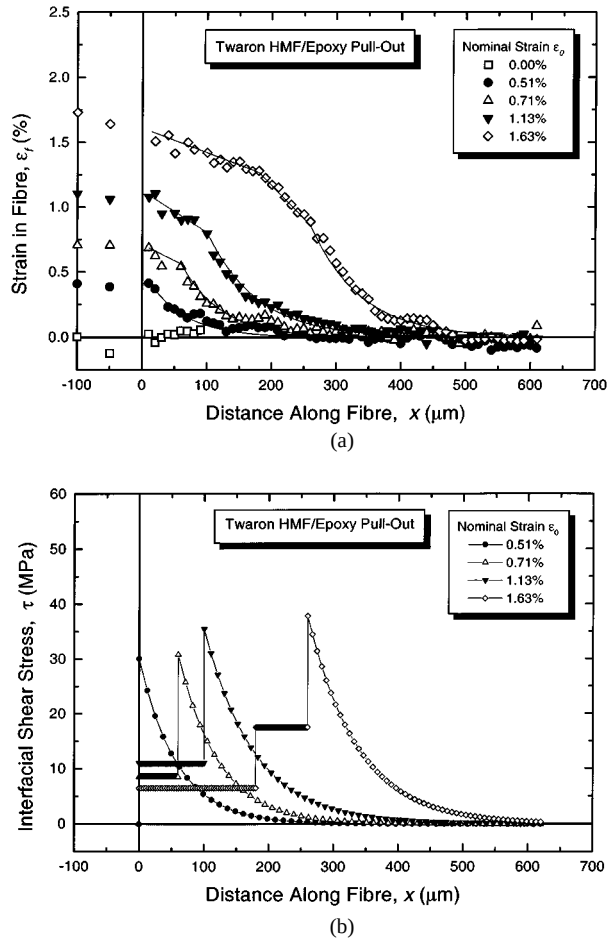

Figure 3 (a) Experimentally-measured and theoretically-predicted variation of fibre strain with distance along the fibre at different nominal strain levels for the Twaron HMF/epoxy specimen with $L_e = 600$ mm undergoing partial debonding. (b) Distributions of interfacial shear stress at different nominal strain levels derived from the data in Fig. 3a.

4.2.2. Surface finished HMF fibres

Fig. 3a shows the axial strain profiles along a Twaron high modulus surface finished fibre of embedded length $L_e = 600$ μm undergoing pull-out from the epoxy resin. As the nominal applied strain is increased above $\varepsilon_o = 0.71\%$ the fibre axial strain profile shows the characteristic linear and shear-lag profiles due to partial debonding. When the nominal strain is increased to $\varepsilon_o = 1.63\%$ the linear region splits into two distinct zones and the transition from linear to non-linear debonded regions of the fibre is difficult to resolve. The application of further stress to the free fibre resulted in the failure of the free fibre. Fit to the partial-debonding theory [5] (Equations 6 and 7) was achieved by adapting the theory to model a number of linear zones defined simply by an x co-ordinate and a suitably chosen value for the frictional shear stress.

Fig. 3b shows the corresponding interfacial shear stress distributions for the HMF sample derived through Equation 3 from the theoretical curves fitted to the fibre strain profile in Fig. 3a. The interfacial shear stresses in the linear region of the interface vary considerably from one zone to another. The first and second linear strain zones are defined by the x co-ordinate values of $m_{(1)}$ and $m_{(2)}$, and by the shear stress values $\tau_{i(1)}$ and $\tau_{i(2)}$. The shear stress of $\sim$17 MPa in the second zone adjacent to the elastic region ($\tau_{i(2)}$) is considerably higher than

TABLE III Interfacial data from 5 Twaron HMF fibre/epoxy resin pull-out specimens

Specimen	ε_o (%)	$m_{(1)}$ (μm)	$\tau_{i(1)}$ (MPa)	$m_{(2)}$ (μm)	$\tau_{i(2)}$ (MPa)	τ_{max} (MPa)
1	0.51					30.2
	0.71	60	8.5			30.8
	1.13	100	11.0			35.4
	1.63	180	6.5	260	17.5	38.7
2	1.20			80	24.0	43.3
	1.55	100	4.0	190	33.0	45.4
	1.84	130	5.0	245	31.0	41.1
	2.52	220	14.0	340	28.0	43.0
3	0.88	100	7.5			40.9
	1.13	120	15.0			46.4
	1.45	150	19.0			36.2
4	0.67					29.9
	0.91	55	10.0			33.0
	1.41	90	7.5	170	21.0	33.3
	1.76	260	11.0			40.2
5	0.67	35	12.0			32.5
	1.01	80	11.0			37.4
	1.19	160	8.3			40.1
Average			**10.0**		**25.8**	**37.7**
SD			**4.0**		**3.9**	**4.0**

the value of ~6 MPa in the first zone ($\tau_{i(1)}$). It should also be noted that the transition from the linear zone 1 to zone 2 occurs at a fibre axial strain of approximately 1.2%. The maximum interfacial shear stress, $\tau_{max}(\equiv\tau_s)$, showed analogous behaviour to the HM samples with an average value of $\tau_{max}^{avg} \sim 35$ MPa. Again this would suggest that the interface fails initially below the shear yield stress of the resin.

Four more Raman pull-out experiments were performed with Twaron HMF fibres and the data obtained were analysed using the partial debonding theory. Two of the specimens also showed the two linear zones and whereas for the other two showed only one linear zone. It was noted, however, that in the two specimens that had only single linear zones the nominal strain did not exceed 1.45%. The interfacial parameters extracted from the Raman plots and theoretical analysis are summarised in Table III. It can be seen that the average maximum shear stress value for the five different specimens, τ_{max}^{avg}, is 37.7 ± 4.0 MPa and the average frictional shear stress τ_i^{avg} is 10.0 ± 4.0 MPa in zone 1 and 25.8 ± 3.9 MPa in zone 2.

4.2.3. Adhesion-activated HMA fibres

Fig. 4a shows the axial strain profiles along a Twaron high modulus surface activated fibre of embedded length $L_e = 1020$ μm undergoing pull-out from an epoxy resin. Only the first 700 μm are presented to magnify the detail around the fibre entrance and enable more accurate application of the partial debonding model.

As the nominal applied strain is increased from $\varepsilon_o = 0.54\%$ to $\varepsilon_o = 1.4\%$ a small region of linear strain initiates in the proximity of the fibre entrance with the transition from linear to non-linear regions of the fibre strain profile difficult to elucidate. The partial debonding theory [5] (Equations 6 and 7) was implemented by iterating the value of τ_i and m giving the least deviation from the experimental data (Excel spreadsheet).

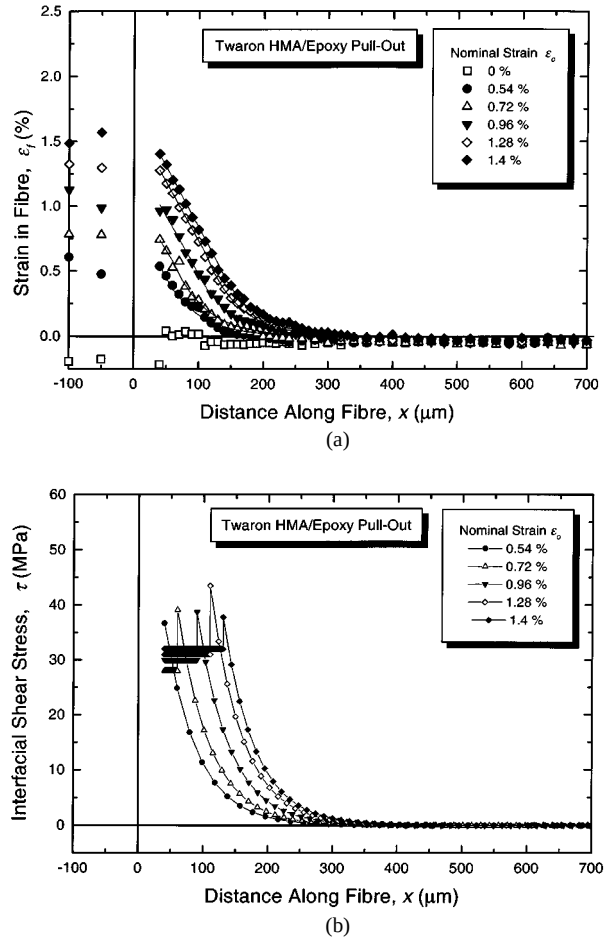

Figure 4 (a) Experimentally-measured and theoretically-predicted variation of fibre strain with distance along the fibre at different nominal strain levels for the Twaron HMA/epoxy specimen with $L_e = 1020$ mm undergoing partial debonding. (b) Distributions of interfacial shear stress at different nominal strain levels derived from the data in Fig. 4a.

The application of further stress to the free fibre, to induce the nominal strain above $\varepsilon_o = 1.4\%$, resulted in the failure of the free fibre outside of the resin block.

Fig. 4b shows the corresponding interfacial shear stress distributions for the HMA sample derived through Equation 3 from the theoretical curves fitted to the fibre strain profiles in Fig. 4a. The interfacial frictional shear stresses in the linear strain region of the interface with have an average value of ~30 MPa are significantly higher than for the HM and HMF aramid fibres described earlier. The maximum interfacial shear stress, $\tau_{max}(\equiv\tau_s)$, was similar to that for the HM and HMF specimens with an average value of $\tau_{max}^{avg} \sim 40$ MPa.

Three further Raman experiments were performed with Twaron HMA fibres and the data obtained also analysed using the partial debonding theory. The interfacial parameters extracted from the Raman plots and theoretical analysis are summarised in Table IV. The values of τ_{max}^{avg} were all very similar at 38.6 ± 3.6 MPa whereas the frictional shear stress values showed significant variability at 22.4 ± 7.5 MPa, indicating the diversity of failure phenomenon that can occur during the pull-out test.

4.3. Failure mechanisms

The epoxy resin blocks and aramid fibres were examined after pull-out testing using scanning electron

TABLE IV Interfacial data from 4 Twaron HMA fibre/epoxy resin pull-out specimens

Specimen	ε_o (%)	m (μm)	τ_i (MPa)	τ_{max} (MPa)
1	0.54			
	0.74	60	28.0	39.1
	1.00	90	30.0	38.7
	1.27	110	31.0	43.5
	1.40	130	32.0	37.8
2	0.87	100	10.0	43.2
	1.22	190	12.0	42.1
	1.60	290	13.0	38.8
3	0.80			
	0.94	70	19.0	33.4
	1.36	85	27.8	39.9
	1.51	100	23.0	40.0
4	0.79			
	0.88	112	15.0	31.3
	1.23	100	22.5	33.4
	1.51	110	28.0	39.6
	1.67	110	22.0	39.8
Average			**22.4**	**38.6**
SD			**7.5**	**3.6**

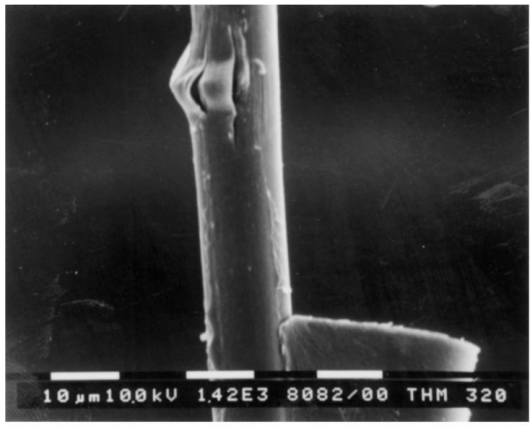

(a)

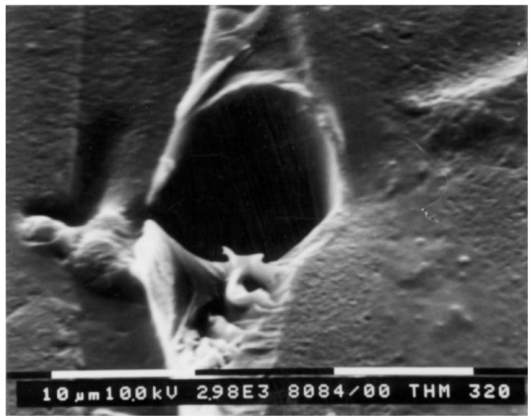

(b)

Figure 5 SEM micrographs of a Twaron HM pull-out specimen after failure. (a) Extracted fibre and (b) cavity left in the epoxy block.

microscopy and significant differences were found for the specimens made using the three different fibres.

4.3.1. As-spun HM fibres

Fig. 5a shows a pulled out fibre HM fibre and Fig. 5b shows the corresponding hole left in the block after extraction of the fibre. Analysis of the extracted fibre reveals a smooth surface unchanged from the topography of the as-received HM fibre shown in Fig. 1a. It can also be seen that there is a clean hole in the epoxy block and there is no evidence of aramid or epoxy debris in the vicinity of the hole. These micrographs are consistent with the strain profiles determined using Raman spectroscopy and imply that the mechanism of failure is debonding of the fibre with very little evidence of plastic deformation of the matrix having taken place and the fibre remaining essentially intact.

The localised damage on the side of the fibre has taken place at the point where the fibre emerged from the epoxy block ($x = 0$). It is probably due to the radial stresses that are thought to be present due to the complex state of stress at the position where the fibre leaves the block [23]. These complex state of stress may also be responsible for the peaks in axial fibre strain that are often found [24] at $x \sim 0$ and can be seen in Fig. 2a.

4.3.2. Surface-finished HMF fibres

Fig. 6a shows a micrograph of an extracted HMF fibre which has a significant variation in surface topography. One side of the fibre shows considerable roughness or damage whilst the other is relatively unaffected. Fig. 6b is a micrograph of the hole left in the epoxy resin block after extract of the HMF fibre. The hole appears to contain the remnants of the extracted fibre in the form of a uniform shell with a thickness of approximately 1 μm. Also present are fibrils that might be associated with the morphology of the aramid skin [25].

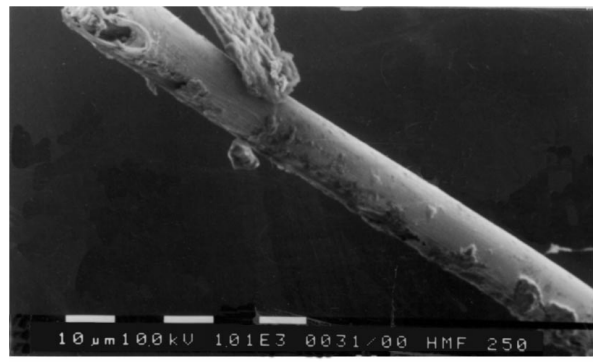

(a)

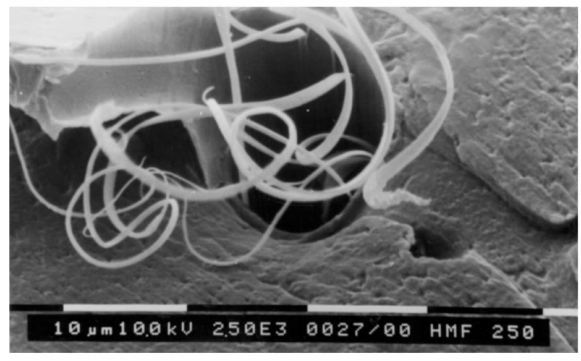

(b)

Figure 6 SEM micrographs of a Twaron HMF pull-out specimen after failure. (a) Extracted fibre and (b) cavity left in the epoxy block.

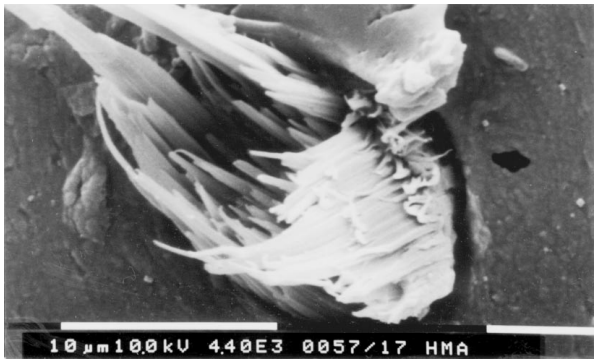

Figure 7 SEM micrograph showing fibre fracture at the point where an HMA fibre entered the epoxy block.

From consideration of the extracted fibre and hole debris it would appear that the interface between the fibre and the finish has completely failed and in addition in some regions the fibre skin have been detached from the core. This failure mechanism would seem to be appropriate when considering adhesion mechanisms at the interface. The increase in surface roughness due to the finish will promote better adhesion [3]. The fibre/finish interface could be considerably weaker than the finish/epoxy interface [12]. There is also another potential interface between the fibre skin and core which is controlled by hydrogen bonding [12]. The strength of these interfaces may vary from one region to another or at different stress levels allowing a combination of failure processes to take place. This is consistent with both the complex state of damage seen in Fig. 6, the fibre strain distributions in Fig. 3a and the variability of interfacial shear stress in the debonded regions found in Fig. 3b and Table III.

4.3.3. Adhesion-activated HMA fibres

It was found that for every HMA specimen tested failure occurred by fracture of the fibre at the point where it emerged from the epoxy block as shown in Fig. 7. The strain distributions in Fig. 4a also showed no evidence of debonding due to the strong interface produced by adhesion activation of the fibre. It appears therefore that fibre fracture is then always initiated by the axial fibre stress concentration at the fibre entrance point that is predicted by finite element analysis [23].

4.4. Comparison of behaviour of fibres with different coatings

At this point it is of interest to compare directly the effect of the presence of the different fibre surface treatments upon the interfacial behaviour of the pull-out specimens. Fig. 8 shows a comparison of the strain distributions in the different fibres at the maximum levels of applied strain in each case. It can be seen that the strain decays rapidly with distance along the fibre for the HMA fibre and more slowly for the HM fibre, with the HMF fibre showing intermediate behaviour. This is a clear indication that the surface treatment of the HMA fibre leads to a greater resistance to interfacial breakdown.

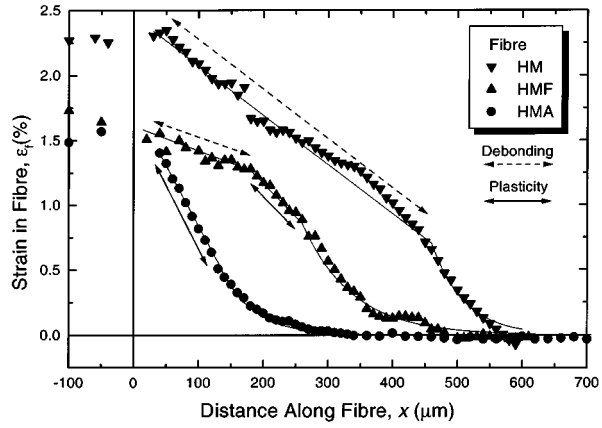

Figure 8 Experimentally-measured and theoretically-predicted variations of fibre strain with distance along the fibre at the highest strain levels for the Twaron HM, HMF and HMA fibres. The possible deformation mechanisms are also indicated (Data taken from Figs 2–4a).

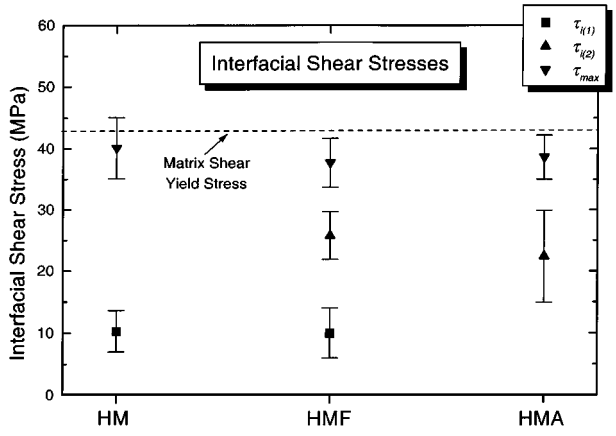

Figure 9 Average values of interfacial shear stress parameters for pull-out specimens made using the different Twaron fibres (Data taken from Tables II–IV).

The average values of the different interfacial shear stress parameters taken from Tables II–IV are shown in Fig. 9 for the three different fibres. There are several points to note. Firstly the values of $\tau_{max}(\equiv\tau_s)$ are similar for all three fibres and just below the shear yield stress of the resin matrix. The important implication of this observation is that the strength of the interface is limited by the shear yield stress of the resin which cannot be exceeded. This is a widely-observed finding for micromechanical testing through the use of Raman spectroscopy [4, 5, 19–21]. Secondly, the lower value of τ_i for HMF is similar to τ_i for HM and the upper value is similar to τ_i for the HMA fibre. The implies that the HMF fibre shows a mixture of interfacial failure processes found for the HM and HMA fibres. Thirdly, the value of τ_i for the HM fibre (Table II) is very low and in combination with the observations of the failure process shown in Fig. 5 implies that debonding occurs in this system at an interfacial frictional shear stress of the order of 10 MPa which is again similar to the value determined for a similar system using other methods [19, 21].

Finally, the value of τ_i for the HMA fibres of around 25 MPa is relatively high and, although the data in Fig. 4 have been fitted to the partial debonding theory, there is no evidence from Fig. 7 of debonding for this fibre. There are, however, linear regions in the strain

distributions shown in Fig. 4a and it appears that these may be regions where shear yielding of the resin has taken place at the fibre/matrix interface. The value of τ_i is significantly lower than the shear yield stress of the matrix (~43 MPa) and may be controlled by the strain-softening of the matrix following shear yielding [26] or plastic deformation within an interphase (the fibre was coated with an epoxy-based finish). These findings are important in the design of better techniques of interfacial modification for high-performance fibres since it appears that even when interfacial debonding can be suppressed completely the strength of the fibre/matrix interface will be controlled by the matrix or interphase properties.

5. Conclusions

- It has been demonstrated that a combination of Raman spectroscopy with scanning electron microscopy is an excellent method of evaluating the effect of surface treatment upon the properties of the fibre/matrix interface for aramid fibres in an epoxy matrix.
- Using the 'partial debonding model' developed by the authors, the strain profiles along the fibres deduced from the Raman measurements have been interpreted in terms of the interfacial shear strength, τ_s and the interfacial frictional stress, τ_i.
- The untreated fibre HM has been found to be characterised by $\tau_s = 40.1 \pm 5.0$ MPa and $\tau_i = 10.3 \pm 3.3$ MPa. The low value of frictional shear stress correlates with smoothness of the fibre observed using SEM. Total fibre pull-out has been observed at strains $\varepsilon_f \approx 2.3\%$. It appears that adhesive failure between the fibre and the matrix is responsible for the interfacial failure.
- The activated fibre HMA is similar the HM fibre in terms of its interfacial shear strength with $\tau_s = 38.6 \pm 3.6$ MPa. It differs, however, in its frictional characteristics being much higher with $\tau_i = 22.4 \pm 7.5$ MPa. This may be due to matrix or interphase shear yielding rather than frictional sliding since the HMA fibre could not be extracted from the epoxy matrix as it failed cohesively at relatively low fibre strains.
- The finished fibre HMF seems to exhibit all of the features found for the HM and HMA fibres. The interfacial shear strength was close to the shear yield stress of the matrix $\tau_s = 37.7 \pm 4.0$ MPa and a combination of adhesive/cohesive failure processes were responsible for two levels of the interfacial frictional stress determined ($\tau_i = 10.0 \pm 4.0$ MPa and 25.8 ± 3.9 MPa). This intermediate behaviour is further vindicated by the fibre morphology observed by SEM with its enhanced fibre roughness, variation in surface topology, and fibrillation and fibre deskinning seen following pull-out.

Acknowledgements

This work was supported by Research Grants from the Engineering Research Council and Shell Research. One of the authors (R.J.Y.) would like to thank the Royal Society for support in the form of the Wolfson Research Professorship in Materials Science. Another (I.A.) is grateful to the Government of Malaysia for financial support.

References

1. P. J. HERRERA-FRANCO and L. T. DRZAL, *Composites* **23** (1992) 2.
2. D. HULL, "Cambridge Solid State Sciences" (Cambridge University Press, Cambridge, 1981) p. 38.
3. J. KALANTAR and L. T. DRZAL, *J. Materials Science* **25** (1990) 4186.
4. A. K. PATRIKIS, M. C. ANDREWS and R. J. YOUNG, *Composites Science and Technology* **52** (1994) 387.
5. D. J. BANNISTER, M. C. ANDREWS, A. J. CERVENKA and R. J. YOUNG, *Composites Science and Technology* **53** (1995) 411.
6. S. L. CHATZI, S. L. TIDRICK and J. L. KOENIG, *J. Polymer Science* **26** (1988) 1585.
7. R. E. ALLRED, E. W. MERRILL and D. K. ROYLANCE, "Handbook of Composites" (Van Nostrand Reinhold, New York, 1982) p. 333.
8. Y. WU and G. C. TESORO, *J. Applied Polymer Science* **31** (1986) 1041.
9. L. S. PENN, T. J. BYERLEY and T. K. LIAO, *J. Adhesion* **23** (1987) 163.
10. C. T. CHOU and L. S. PENN, *J. Adhesion* **36** (1991) 125.
11. K. W. ALLEN, *J. Adhesion* **21** (1987) 264.
12. J. MAHY, L. W. JENNESKENS and O. GRABANDT, *Composites* **25** (1994) 653.
13. J. KALANTAR and L. T. DRAZL, *J. Materials Science* **25** (1990) 4194.
14. P. S. CHUA and M. R. PIGGOTT, *Composites Science and Technology* **22** (1985) 33.
15. M. R. PIGGOTT, "Load Bearing Fibre Composites" (Pergamon Press, Oxford, UK, 1980) p. 83.
16. A. KELLY and N. H. MACMILLAN, "Strong Solids," 3rd ed. (Clarendon Press, Oxford 1980).
17. M. DESAEGER, I. VERPOEST, T. LACROIX, B. TILMANS and R. KEUNINGS, *Composites Science and Technology* **43** (1992) 379.
18. C. H. HSEUH and P. F. BECHER, *J. Materials Science Letters* **12** (1993) 1933.
19. M. C. ANDREWS, R. J. YOUNG and J. MAHY, *Composites Interfaces* **2** (1994) 433.
20. M. C. ANDREWS, R. J. DAY and R. J. YOUNG, *Composites Science and Technology* **48** (1993) 255.
21. M. C. ANDREWS, Ph.D. thesis, UMIST, 1994.
22. M. C. ANDREWS, D. LU and R. J. Young, *Polymer* **38** (1997) 2379.
23. C. MAROTZKE, *Composite Science and Technology* **50** (1994) 393.
24. D. J. BANNISTER, Ph.D. thesis, UMIST, 1996.
25. R. J. MORGAN, C. O. PRUNEDA and W. J. STEELE, *J. Polymer Science: Polymer Physics Edition* **21** (1983) 1757.
26. D. TRIPATHI and F. R. JONES, *J. Materials Science* **33** (1998) 1.

Received 6 January
and accepted 22 July 1999